J Math Chem (2012) 50:2061–2085
DOI 10.1007/s10910-012-9995-8

ORIGINAL PAPER

Topography of cyclopropyl radical ring opening to allyl radical on the CASSCF(3,3) surface: valley-ridge inflection points by Newton trajectories

Wolfgang Quapp · Josep Maria Bofill

Received: 9 January 2012 / Accepted: 15 March 2012 / Published online: 5 April 2012

Abstract Valley-ridge inflection points (VRI) on the potential energy surface for the ring opening of the cyclopropyl radical to the allyl radical are determined using the tool of Newton trajectories (NTs) (Quapp and Schmidt in Theor Chem Acc 128:47, 2011). The UHF surface is treated in a former paper (Quapp et al. in Theor Chem Acc 129:803, 2011). This paper is the extension to the more expensive CASSCF(3,3) surface. We compare the results on the UHF surface with the more appropriate calculation: there are quantitative as well as qualitative changes, of course. But many fundamental relations are the same on both surfaces. However, we could detect new pathways on the CASSCF(3,3) surface which highlight the bifurcation problem of this radical. VRIs play a role in the understanding of bifurcating reactions. The region where the bifurcation takes place is governed by a VRI point. Because the transition state of the ring opening is not symmetric, the steepest descent (SD) from the transition state is not along a symmetry axis either, and in this case the SD usually fails a downhill VRI point. The SD from the transition state of the ring opening goes to the disrotatory minimum of the allyl radical. In contrast, we find some pathways which end at the conrotatory minimum, and which go along so-called non steepest descent paths, at least in parts. The region of interest (around the SP of the ring opening) is crossed by electronic intersection seams. Conical intersection points on the seam can

W. Quapp (✉)
Mathematisches Institut, Universität Leipzig, PF 100920, 04009 Leipzig, Germany
e-mail: quapp@uni-leipzig.de
URL: www.mathematik.uni-leipzig.de/MI/~quapp

J. M. Bofill
Departament de Química Orgànica, Universitat de Barcelona,
c/Martí i Franqués, 1, 08028 Barcelona, Spain

J. M. Bofill
Institut de Química Teòrica i Computacional, Universitat de Barcelona (IQTCUB),
c/Martí i Franquès, 1, 08028 Barcelona, Spain

be detected by NTs. We use the possibility to explore parts of the intersection seam of the lower CAS surface and we determine connected VRI points being the corner stones of the possible ring opening channels in the disrotatory and the conrotatory case.

Keywords Valley-ridge inflection point · Newton trajectory · Reaction bifurcation · Ring opening of the cyclopropyl radical · Disrotatory and conrotatory case

1 Introduction: the theory of Newton trajectories and bifurcation points

The concepts of Potential Energy Surface (PES), Reaction Path (RP) and its more restrictive definition Minimum Energy Path (MEP) are the basic grounds of many theoretical chemistry theories and models [1,2]. The RP is defined as a continuous curve in the coordinate space, which connects two minimums of the PES by passing through a first order saddle point (SP), also called transition structure (TS) of the PES. The energy of the SP is assumed to be the highest value tracing along the RP. The putative MEP used by many chemists and well-defined is the intrinsic reaction coordinate (IRC) [3], which is the path of steepest descent (SD) in mass-weighted Cartesian coordinates. Note that it can be used with an independent definition [4,5]. The IRC could be assumed to be a trajectory with its kinetic energy removed after each infinitesimal step. However, this does not protect the IRC against to use a ridge pathway instead of a valley nearby, like it is demonstrated in a simple example [6]. If one understands the MEP to be a valley way throughout, than such an IRC is not an MEP. It only meets the general RP definition. Another special definition of an RP is the reduced gradient following (RGF) [7–14] and its equivalent definition, the so-called Newton trajectories (NT) [15,16]. Short defined, it is a curve where at every curve point the gradient points into the same direction, the so-called search direction. If the NT is completely located in a valley region, up to the SP, then this RP meets also the category of an MEP [17].

In Fig. 1 we see erosion rills. The reader should translate this surface to a picture of a PES and should ask: "what is here the MEP?" In a next step he, or she, should extend such a PES to seven or more degrees of freedom in the configuration space of a molecule. We believe that the PES of the allyl radical is somehow channelized. We think that SD calculations only cannot give a full picture of the PES.

An important feature of the PES is that a valley or a ridge can bifurcate. The fact is related to the existence of a valley-ridge inflection (VRI) point [15]. A VRI point is a point in the configuration space where, orthogonally to the gradient, at least one main curvature of the PES becomes zero. The gradient itself is assumed to be not the zero vector. The VRI points can be classified into different main classes. A valley starting from an SP can bifurcate downhill and the two branches can lead to two valleys with their corresponding minimums. Between the two valleys a ridge emerges. Then the VRI point is a valley-pitchfork (vpVRI) bifurcation. Or, a valley starting from a minimum can bifurcate uphill and the two branches lead to two SPs. Between the two valleys again a ridge emerges usually leading to an SP of index two. Then the VRI point is also a vpVRI bifurcation. There is another possibility that a ridge on

Fig. 1 Deep erosion furrows of distinctive charm, on a ridge. Photo of the "badlands" on the southern slope of the Castle Wachsenburg in Thüringen, Germany, with its colorful Keuper marl clay. Permission of Manfred Müller, Gotha, http://home.fotocommunity.de/kartenmanfred

the PES bifurcates into two ridges, and between the two ridges emerges a valley. The VRI point is a ridge-pitchfork (rpVRI) bifurcation. A further mathematical possibility, which is not as interesting from the point of view of chemistry, is that in between a ridge of index 2 emerges—in cases with a PES of more than two dimensions. A next possibility is that the VRI point is of a valley-ridge touching kind. The last possibility is the border-line case due to flat branches. So to say, its character is of a mixed type [15,18]. The possibilities, vpVRI and rpVRI, as well as the mixed type, will emerge on the CASSCF(3,3) PES of the cyclopropyl radical ring opening, which is analyzed throughout the article. The case is not discussed in the paper, that VRI points can form a connected manifold [19–21].

We could not make useful "optimized" 2-dimensional PES scans for this very floppy molecule, even not from the ground state. Like in the 1-dimensional case of a distinguished coordinate on the famous Müller-Brown surface [22], here, an optimization over a 2-dimensional raster of points results in a picture where crossing a certain curve the energy jumps, but does not change continuously between the corresponding raster points. However, NTs are continuous curves. So, we try to fire our imagination of the PES of the cyclopropyl radical ring opening by pictures of projections of NTs into different 2-dimensional planes. Using additionally the eigenvalues of the Hessian, we can report the valley- or ridge character of the current region of the PES which the NT explores. In this kind we will try to understand the region between the global SP_{ca} of the ring opening and the different allyl radical minimums, as well as the barrier between the minimums by NTs.

An NT can be calculated by an Euler-Branin-step method following along the direction of the vector field $\mathbf{Ag}$ of the so called Branin differential equation [23]

$$\frac{d\mathbf{x}}{dt} = \pm\mathbf{A}(\mathbf{x})\mathbf{g}(\mathbf{x}), \tag{1}$$

where **A** is the adjoint matrix to the Hessian, and **g** is the gradient of the surface. **x** is the current point, and t is a curve length parameter. A second definition of the NT is given by the projector equation

$$\mathbf{P_r g}(\mathbf{x}(t)) = \mathbf{0}. \tag{2}$$

The projector can be defined by a dyadic product with a normalized search direction, **r**

$$\mathbf{P_r} = \mathbf{E} - \mathbf{r}\,\mathbf{r}^T\,, \tag{3}$$

where **E** is the unit matrix. The curve can be calculated numerically by the derivation of the projector equation along the curve parameter t giving also the tangent of the NT [9]. The Eq. (2) means that along an NT the gradient always points into the **r**-direction.

Between a minimum and an SP of index 1 there are infinitely many regular NTs. However, the theory says, that between a minimum and an SP of index 2 one singular NT exists which also crosses the VRI point which has to be in between. In reference [24], an iteration is proposed to find exactly the one singular NT using an empirical variational approach. We use the method throughout this article. The reader should look for the details there. With an initial choice of a search direction we calculate by predictor- and corrector steps an NT starting from a minimum or an SP into the region of the guessed VRI. Sometimes the corrector does not work well close to the VRI region. Then we only use predictor steps for an approximated quasi-NT. NTs are continuous curves. Their calculation discretizes the curve into a set of nodes in certain distances, so to say, the nodes are points of support of the NT. The steplength of the predictor step prescribes the distance between the nodes. Connecting all nodes of the NT with the guessed VRI and dividing the lines into further test points, we test for all these points the value of norm $|\mathbf{A}\,\mathbf{g}|$ and use the node with the minimal value for the new VRI point. Note that at the VRI point holds $|\mathbf{A}\,\mathbf{g}| = 0$ [8]. The adjoint matrix, **A**, to the Hessian is used, and **g** is the covariant gradient of the PES. The gradient at the guessed VRI is then used for the new search direction for a new NT run, starting at the guessed new VRI, and so on, up to convergence. Of course, the key is always an appropriate guess of the VRI region at the beginning. The method is coupled with the GAMESS-US program [25–27] for the CASSCF(3,3) calculation of energy, gradient, Hessian matrix and metric matrices in non-redundant, internal z-matrix coordinates. All this is used at every node without any updating, see also web-page [28] for the programs of the VRI-propose [24].

2 Thermal ring opening of cyclopropyl radical into allyl radical

In Organic Chemistry and Chemistry in general, the prediction of the stereochemistry of the electrocyclic ring-opening reactions, such as the cyclopropyl radical, has been a long-standing question. For cyclic molecular structures in their ground state with an even number of electrons these reactions are governed by the Woodward-Hofmann rules [29–31]. These rules predict either a conrotatory or disrotatory stereochemistry

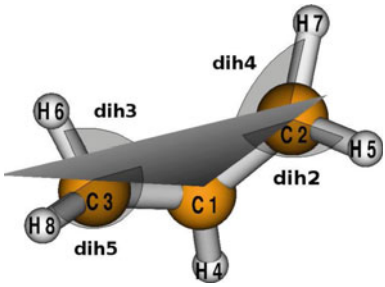

Fig. 2 Ring opening of the cyclopropyl radical: numbering of atoms in the z-matrix

```
cyclopropyl radical <--> allyl radical
C1
c1
c2  1  r1
c3  1  r2   2  c2c1c3
h4  1  hc1  2  hcc1   3  dih1
h5  2  hc2  1  hcc2   3  dih2
h6  3  hc3  1  hcc3   2  dih3
h7  2  hc4  1  hcc4   3  dih4
h8  3  hc5  1  hcc5   2  dih5
```

evolution depending on the orbital diagram associated to the system. For the cyclopropyl radical, a system with an odd number of electrons, the Woodward-Hofmann rules predict that both the conrotatory and disrotatory stereochemistry evolution are nominally forbidden [32]. In the computational study reported in reference [32], a highly asynchronous TS with C_1 symmetry was identified. In a later computational study at the B3LYP/6-311G(2d) level of theory [33], the calculations of the RP represented as Intrinsic Reaction Coordinate (IRC) were carried out from the C_1 transition state to the allyl radical, concluding that the overall reaction occurs with disrotatory stereochemistry. Nevertheless, it is not possible to conclude from the IRC study alone, that when starting at an asymmetric TS, the disrotatory stereochemistry is favored. To clarify this question Mann and Hase carried out dynamical calculations [34,35]. The study was carried out with a limited number of trajectories, but the authors conclude that with a large ensemble of trajectories one may predict no stereochemical preference for the ring opening. To explain this result, the authors argue that the possible existence of a VRI point along the PES region is associated to the ring opening process. Recently, an IRC analysis of this reaction concludes that there exists a VRI point near the IRC curve, and this VRI point is located on a ridge that divides the SP valley in two valleys, each one related to the allyl radical [36]. In the foregoing paper [37], hereafter referred as part I, we confirmed this VRI point. However, this VRI point is on a very skew ridge and SD curves do not bifurcate there. Thus, the question is unsolved which SD pathway could lead to the conrotatory minimum. Additionally, we detected in part I a possibility of an RP over a further VRI point at a side flank of the UHF PES, which leads to an SP with a connection to the two different allyl radical minimums. Thus, we could propose a bifurcation of a post SP-RP into the disrotatory or conrotatory case.

Table 1 CASSCF(3,3)/6-31G(d,p) coordinates of minimum M_c, VRI_c and SP_{ca} sorted in the order of the z-matrix, see Fig. 2

M_c (−116.432094 au)			VRI_c (−116.390855 au)			SP_{ca} (−116.394201 au)		
1.4720			1.4466			1.4070		
1.4994	61.381		1.4473	92.440		1.4732	90.388	
1.0722	129.438	−119.428	1.0629	120.581	−129.238	1.0752	121.156	−127.568
1.0782	118.656	108.212	1.0758	120.598	109.044	1.0788	123.633	119.367
1.0773	118.357	106.395	1.0751	121.572	83.777	1.0732	121.469	80.697
1.0775	118.311	−106.987	1.0751	121.540	−83.635	1.0737	119.992	−65.821
1.0777	118.723	−107.603	1.0758	120.571	−108.940	1.0736	120.069	−91.222

The energy is reported in brackets (), see Fig. 16 below

The energy of the highest point of that path was only slightly over the energy of the global TS of the ring opening.

In the same kind like in part I, the atoms numbering is given in Fig. 2. This and the z-matrix are used throughout the present study. In the z-matrix, the distances are given in Å and angles and dihedrals in degree.

The purpose of the present study is again both, to show the potentiality of the NTs as a tool to view and analyze a PES, and to compare the results of part I with detailed features of the CASSCF(3,3)-PES with 6-31G(d,p) basis set (complete active space) [38–42] related to the ring opening of the cyclopropyl radical, being the active space selected according to that explained in references [43,44]. Briefly, the CASSCF theory is based on the multiconfigurational self-consistent field method where the wave function includes all possible configurations of a limited set of orbitals and electrons, the "active space". In fact it is possible to select a set of active orbitals and electrons and consider zeroth-order correlation in this space only.

The wave functions of the known minimums of the cyclopropyl and the allyl radicals are shown in Figs. 1 and 2 of part I. The internal coordinates are reported in Table 1 and in Table 4 below following the z-matrix of Fig. 2. (Note that in this ansatz of the CASSCF the cyclopropyl radical minimum, M_c, is not perfectly symmetric. The reason is that the initial or guess CASSCF wave function is not adapted to the C_s symmetry. We remember that the minimum of cyclopropyl is C_s. The double precision calculations like GAMESS-US set the wave function to convergence at 10^{-8} implying that the distances are correct up to the third digit and the angles up to the second digit. With these two considerations the symmetry problem can be solved.) We get the given result in a direct minimization by GAMESS-US, as well as in a very fine SD search. A CAS calculation with QUAD = .TRUE.(quadratic optimization method for orbital and configuration interactions coefficients) results in a full symmetric geometry (not given in Table 1). The CASSCF(3,3) minimization by GAMESS-US is the optimum active space according to Pulay et al. [43,44] procedure to reach the minimum M_c or the allyl radical minimum, M_a, structures. However, larger active spaces can be used but the results are the same [45]. On the other hand, the M_a minimum could be reached in a fully symmetric form for an SD calculation which finds the C_{2v} symmetry. The CASSCF(3,3) minimization by GAMESS-US also gives here a slightly asymmetric

geometry. However, that asymmetry is very small, and does not have any influence on the reported results of this paper based in the exploration of the PES by the NT method; especially for NTs which end at the minimums.

As explained in reference [32], it is important to analyze at different points of the PES the expectation value of the spin-squared operator S^2, $\langle S^2 \rangle$, of the wave function. This magnitude in the present system indicates the spin contamination of states of higher multiplicity (i.e. quartet, sextet, …) to the doublet state multiplicity. Normally, in the points of the PES where $\langle S^2 \rangle$ differs from the value of the pure doublet wave function, namely 0.75, the UHF wave function shows a spin contaminant mainly due to the quartet state. If one uses the single-configuration approach, then the wave function of the quartet state can be written as a linear combination of three Slater determinants where each determinant is characterized by three molecular orbitals. These three molecular orbitals are related in some way to the σ double-occupied, n single-occupied, and σ^* un-occupied of the cyclopropyl molecular orbital system, see Fig. 1 of part I, and to the π_1 double-occupied, π_2 single-occupied, and π_3 un-occupied orbitals of the allyl π-molecular orbital system, see Fig. 2 of part I. The σ and σ^* molecular orbitals are related to the CC bond of the cyclopropyl radical to be broken in the evolution to the allyl radical, they are located in this bond, whereas the n orbital is the single occupied molecular orbital located at the methine group, -C1H4, of the cyclopropyl molecular system.

According to this, the ring opening system is minimally well described by three electrons and three orbitals, whereas the remaining electrons act as a core potential. The CASSCF wave function capable to describe this reaction adequately should be constructed using three electrons distributed within the above three molecular orbitals and the remaining electrons act as spectators [32]. A reasonable rule of thumb is that any orbital having an occupation number greater than 1.98 or less than 0.02 is not important enough to be included in the CAS space [46]. For this molecule, usually 13 orbitals are the interesting ones. Nevertheless, in the study of part I we have found regions where the electronic description above is not enough, where in addition to the three mentioned electrons some core electrons are necessary to obtain a correct electronic description. It concerns the electronic intersection seam of the ground state with the PES of an excited electronic state. The Born-Oppenheimer approximation assumes that the electrons instantaneously relax to their lowest energy distribution. For intersecting PES's the situation becomes different. Because the electrons are strongly quantum mechanical, the transition cannot be a slow "cooling" but has to be an ultrafast process that occurs at molecular geometries where the electronic states are isoenergetic [47,48]. The geometries constitute a conical intersection and can be thought of as the TS in the relaxation of the electronic excited molecule. However, these are not isolated points. They are rather collections of geometries that form a higher dimensional seam [49,50].

3 The cyclopropyl radical bowl

The cyclopropyl radical minimum, M_c, at CASSCF(3,3)/6-31G(d,p) level of theory is well known, see Table 1. The index c is used for points of the cyclopropyl part. This

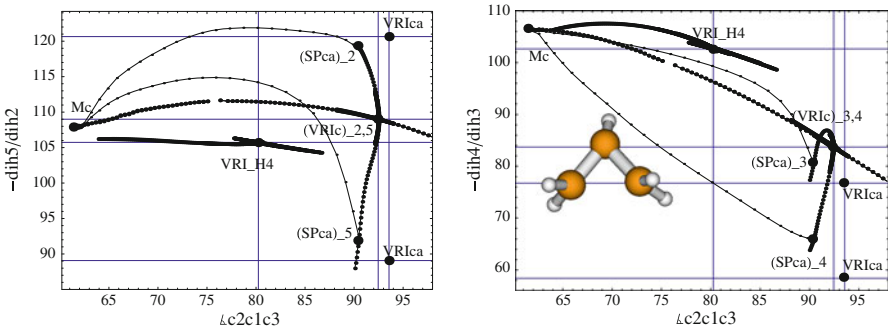

Fig. 3 The VRI point, VRI_c, of the "pre"-transition-state symmetry break for the ring opening of the cyclopropyl radical indicated by the singular NT (*fat nodes*) and its bifurcation point, see text. One cross of *grid lines* is the exact location of VRI_c. *Left*: the representation uses the doubling of all points for coordinates dih2, as well as −dih5, to the same bond angle coordinate C2C1C3. *Right*: The same singular NT through VRI_c for coordinates dih3 and −dih4. The *inlay* is the geometry of the symmetric VRI_c. Additionally shown are three branches of the singular NT through VRI_{H4} for the movement of the single methine, H4, and the location of the past-SP VRI_{ca}. A direct, regular NT connects M_c and SP_{ca} (*thin nodes*)

geometry structure belongs to the C_s point group of symmetry, and due to this fact the distance r1 is equal to r2 and the dihedral angles satisfy the relation dih2 = −dih5 and dih3 = −dih4. With the dihedral that involves the H4 atom, this set of coordinates is the relevant in the changes of the molecule under the ring opening. The remainder of pairs of geometry parameters also preserves the C_s symmetry relation. The numbering of the two methylenes is interchangeable. Thus, in this study we will treat the corresponding pairs of coordinates throughout.

From the minimum M_c two "reaction directions" emerge. One is the 1-dimensional transit of the single methine hydrogen, H4, through the symmetry plane of the carbons, thus the dihedral angle goes through ±180° [51,52]. There is an SP_{H4} of the PES, see Table A2 of part I. The CAS case is quite analogous to the UHF case in part I.

The other possibility is the ring opening of the M_c structure by an increase of the angle C2C1C3, which is equivalent to the bond breaking C2C3. The bond angle C2C1C3 will be like a reaction coordinate in this paper. The reaction should start in the symmetric subspace of all corresponding coordinate pairs of minimum M_c, thus there is, at least a 3D, subspace of important possibilities for the pairs r1 = r2, dih2 = −dih5, and dih3 = −dih4. Note that the z-matrix has 18 internal coordinates which we can decompose as follows, seven pairs each pair being related by the C_s symmetry, the C2C1C3 bond angle and the three coordinates of the H4 atom. The search for the symmetry breaking point VRI_c can start with the template of the UHF surface; however, the search is not successfull. It emerges that the point VRI_c is located "slightly behind" the C2C1C3 angle of the SP_{ca}, see Fig. 3. It has also a slightly higher energy than the SP_{ca}. An analysis of the branches shows that its character has changed, against VRI_c on the UHF surface. Now it is an rpVRI point. The valley from M_c in the symmetric space ends, a ridge of index one uphill in the symmetric space starts, like on the UHF surface, however, the side branches are mild ridges downhill to the SP_{ca}. The something weird VRI point was found under the search for the other VRI_{H4} point depicted also in Fig. 2; its coordinates are given in Table 2.

Table 2 Coordinates of VRI_{H4}, an SP of index two, and VRI_{ca} (with energy)

VRI_{H4} (−116.392025 au)			SP_{i2} (−116.260647 au)			VRI_{ca} (−116.394942 au)		
1.4589			1.4123			1.4018		
1.4594	80.177		1.4124	85.297		1.4877	93.543	
1.0729	130.623	−138.702	1.8672	108.4604	−107.897	1.0735	122.626	−127.200
1.0762	118.846	105.700	1.0773	118.3910	128.772	1.0881	125.568	120.302
1.0762	120.197	102.690	1.0752	125.9946	53.686	1.0666	124.641	77.363
1.0761	120.152	−102.725	1.0752	126.0026	−53.656	1.0715	119.738	−58.517
1.0765	118.848	−105.741	1.0773	118.3895	−128.769	1.0546	124.179	−88.260

The representation in our figures is the same like in part I. We use both dihedrals, dih2 and −dih5, in one figure, as well as dih3 and −dih4 in one figure (with an exception in Sect. 7). Up to the VRI point the two angles are symmetric, thus it is a single curve of nodes, but after the VRI point, the NT bifurcates and goes through different values and describe the behavior of the unsymmetric reaction path. (If we accept that the singular NT can be a description of an RP. A "good" RP is shown in Fig. 2 by the NT with thin nodes.) We use additional indices for the different special points to represent the corresponding coordinates: $(SP_{aa})_2$ for coordinate dih2, $(VRI_c)_{2,5}$ for the bifurcation of coordinates dih2 and dih5, and so on.

Starting at the minimum, M_c, the singular NT has symmetric nodes up to the valley-ridge inflection point, VRI_c. The pathway is a valley along the ring opening, which ends at VRI_c, and two different ridges go slightly downhill to the two representations of the SP with C_1 symmetry, named SP_{ca}. At the SP we find an asynchronous torsion of the two methylene groups. The central branch of the singular NT goes after VRI_c strongly uphill in energy as a symmetric ridge belonging to the C_s symmetry. Because the two representations of the SP are not symmetric, the pathways leading to them are not symmetric either. The symmetry C_s is lost at the bifurcation point. It is a dramatic difference between the left and the right panel of Fig. 3. The outgoing coordinate paths are not equal. It is necessary to destroy the initial molecular symmetry of M_c to arrive at the corresponding SP_{ca} [32].

The border between the regions where NTs going to SP_{H4}, or others going to an SP_{ca}, is marked by a singular NT which bifurcates at a symmetric bifurcation point in C_s, the VRI_{H4}, see Table 2. It is quite analogous to the UHF case in part I, see Fig.3. Here the bifurcation mainly concerns the coordinate dih1 in a plane with the bond angle C2C1C3. There is experimental evidence that the lone H4 of the C1H4 bond can tunnel through the barrier of SP_{H4}, if the cyclopropyl radical is vibrationally exited [52]. The character of the VRI_{H4} is of the mixed type, thus it is neither vpVRI nor rpVRI.

There exists a fully symmetric SP of index two, SP_{i2}, see Table 2, as well as on the UHF surface, see part I. In Scheme 1 of part I [37] of this study, we collected the complete set of treated relations in the cyclopropyl radical bowl.

4 The SP_{ca} and the VRI_{ca} at the end of the SP valley

The SP_{ca} associated to the ring opening of the cyclopropyl radical into the allyl radical is well known [32]. The coordinates used in the present study are reported in Table 1. The SP is not symmetric like the cyclopropyl or allyl radicals, compare Fig. 3, and the corresponding version in Table 1. After the SP, with a further ring opening, there should be the post-TS bifurcation, because at a possible end of the pathway one expects to find one of the two versions of an SP_{aa} in the allyl radical bowl, here the $(SP_{aa})_{3,5}$ corresponding to the coordinates of Table 3. Its methylene 1 is in the C-plane, but its methylene 2 is turned. Due to this fact a downhill pathway flowing into the $(SP_{aa})_{3,5}$ region from SP_{ca} may be a ridge. At the beginning, the pathway is a valley. As an immediate consequence a VRI point must exist. The VRI_{ca} point was found using the guess of the corresponding UHF case, see Fig. 4.

A picture close to this VRI_{ca} point is that given in Fig. 8 of reference [53]. However, there the side branches of the VRIs are still symmetric. Nevertheless, there are two forks of two singular NTs: the left one is the "usual" case where the two side branches are valley lines going downhill into the next two minimums, but the right fork is this case where the two side branches are ridges going uphill to the next two maximums. Note that a curve system of a singular NT at the VRI point consists of four branches.

In a larger region around the VRI point, the corrector for regular NTs [8,9] does not work. We calculate the given singular NT by predictor steps only using Branin-Euler steps along an equation of the tangent, the so called Branin differential equation (1).

Table 3 CASSCF(3,3) coordinates of $(VRI_{ac})_{3,5}$, $(SP_{aa})_{3,5}$ and $(SP_{aa})_{2,4}$

$(VRI_{ac})_{3,5}$ (−116.452813 au)			$(SP_{aa})_{3,5}$ (−116.466343 au)			$(SP_{aa})_{2,4}$ (−116.466342 au)		
1.3548			1.3230			1.4810		
1.4650	113.418		1.4806	124.907		1.3429	124.587	
1.0759	125.043	−167.324	1.0815	118.542	−180.040	1.0811	116.832	−179.980
1.0734	123.861	163.087	1.0763	121.824	180.0	1.0752	119.865	100.646
1.0630	125.908	90.828	1.0964	119.857	100.134	1.0755	121.220	180.0
1.0700	121.781	−9.109	1.0757	121.277	0.0	1.0752	119.866	−100.669
1.0443	128.735	−99.660	1.0751	120.060	−100.290	1.0760	121.729	0.0

Table 4 CASSCF(3,3) coordinates of $(VRI_{ac})_{2,4}$, VRI_{pp}, and minimum M_a

$(VRI_{ac})_{2,4}$ (−116.448170 au)			VRI_{pp} (−116.365305 au)			M_a (−116.487849 au)		
1.4894			1.5042			1.3916		
1.3590	118.878		1.4541	128.151		1.3916	124.651	
1.0968	113.683	−150.971	1.0790	117.038	−178.051	1.0779	117.679	−180.029
1.0809	114.884	86.108	1.0767	120.289	101.408	1.0735	121.326	180.023
1.0827	118.894	16.688	1.0809	121.192	80.761	1.0717	121.343	179.944
1.0765	124.191	−118.920	1.0745	121.638	−78.925	1.0753	121.216	0.014
1.0580	123.496	−160.578	1.0782	120.733	−80.597	1.0769	121.198	−0.041

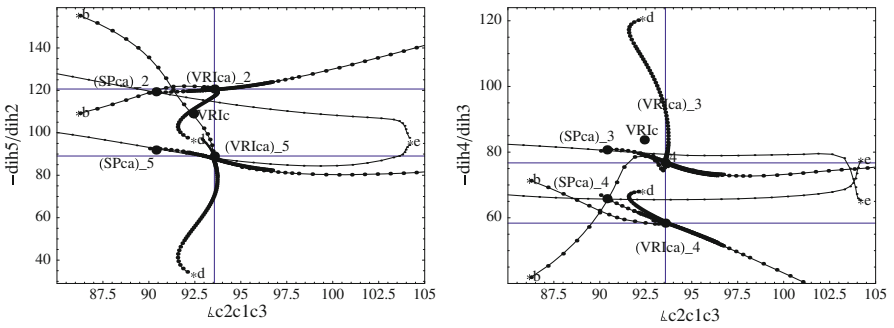

Fig. 4 VRI$_{ca}$ point behind the transition state, SP$_{ca}$, of the ring opening of the cyclopropyl radical. The PES construction is based on the functional energy CASSCF(3,3)/6-31G(d,p). *Left*: pieces of the singular NT through the VRI$_{ca}$. The two different side branches are discernible by a different distance of the nodes. Coordinates: angle between the C-atoms, and the two dihedrals dih2 and −dih5. The cross of the *grid lines* is the location of the VRI point. The ∗ symbol indicates putative CI points. **b* and **d* are end nodes of the side branches of the singular NT. An NT with small nodes is a regular NT to a further putative CI point depicted by the **e* symbol. *Right*: coordinates are the angle between the C-atoms, and the two dihedrals dih3 and −dih4

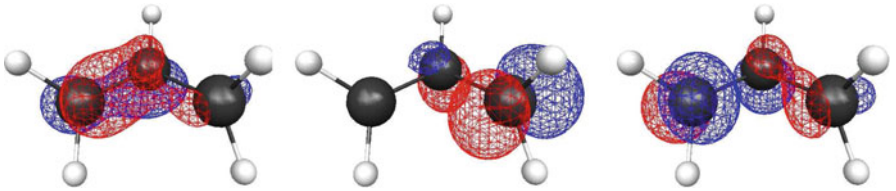

Fig. 5 Geometric structure and CASSCF(3,3) natural orbitals of the VRI$_{ca}$

The differential equation (1) is translated into a difference equation, and a steplength is fixed for steps into tangent direction. Usually, the eigenvalues of the Hessian are small (<1), in the system of internal coordinates in Bohr and radiant used by GAMESS-US, and so the determinant of the 18 × 18-Hessian matrix has a value around 10^{-15}. Its desingularized inverse, the adjoint matrix **A**, could suffer under numerical problems if the determinant of **H** is that small. To avoid this, we multiply all entries of the Hessian by an (arbitrary) factor of 7.5, before we calculate the matrix **A**. That gives values of |**Ag**| in a normal number region. Note that the corrector with its Newton-Raphson steps [8,9] does not work in the region. However, this does not mean to be a breakdown. Because near the VRI point, regular NTs are usually strong curvilinear but the searched VRI is usually outside the convex region. Tangent steps in direction $\mathbf{x}'$ of Eq. (1) along such a curvilinear NT make their approximation error into the 'right' direction. They lead nearer to the VRI point. If the VRI point is reached, the emergence of a cross of branches of the singular NT demonstrates the final success, see Figs. 3 and 4. Of course, predictor-only steps avoid an important number of calculations.

The electronic structure of VRI$_{ca}$ is interesting because it represents the change of the electronic state of the symmetric cyclopropyl structure (the "rabbit ears" of Fig. 1 of part I), and it characterizes the unsymmetric region of the PES. The three natural orbitals are shown in Fig. 5, compare also Fig. 7 of part I.

The pathways of the side branches of VRI_{ca} lead to two putative conical intersection points (CI) depicted by *b and *d, see Fig. 4. (We number the putative CI points by small letters, where 'a' and 'c' are left out to avoid the assignment with the allyl or the cyclopropyl bowls.) The CI seam points are detectable by the value of $|\mathbf{Ag}|$ which increases along the NT into exorbitant values [54]. For the CI point *b, we find $|\mathbf{Ag}| \approx 2{,}250$, caused by a very large absolute value of the first eigenvalue of the Hessian matrix, -6.33. For the CI point *d, we find $|\mathbf{Ag}| \approx 3{,}770$, with the first eigenvalue -6.0. One should compare the $|\mathbf{Ag}|$ value at the VRI point, which should be theoretically zero. It is here at the nearest node 0.0063. Included in Fig. 4 is an additional, regular NT which also leads to a putative CI point. It is drawn with smaller nodes, to allow to see the difference to the singular NT. At point *e we find $|\mathbf{Ag}| \approx 32$, under a milder first eigenvalue of the Hessian of -0.63.

5 The ridge system between VRI_{ca} and the SP_{aa} in the disrotatory case

A VRI system of a singular NT consists of four branches. The character of the single branches determines the character of the VRI point. The character of the VRI_{ca} is a branching of the uphill leading ridge from an hypothetical SP_{aa} region (being at the right hand side, out of Fig. 4) into two side ridges going further uphill, and the one valley in between, which leads to the SP_{ca}, exactly like on the UHF surface in part I. The character is an rpVRI of the chemically "interesting" case: between the bifurcating ridge-branches is the valley. But, the ring opening valley from SP_{ca} downhill ends at the VRI point. There are no bifurcating valleys downhill. Some authors name the situation of such an ending valley a "dangerous" bifurcation [55], or a bifurcation with indeterminate outcome, because further downhill after the VRI point, the one-dimensional valley ground line disappears. After the VRI_{ca} only an "instable" ridge-pathway continues further downhill. The "dynamical" behavior of the molecule becomes indeterminate because no side walls of a valley will lead the reaction. In contrast to the UHF case, the "double bend" of the downhill branch is missing here, near the VRI_{ca} region. It emerges, in a weak form, nearby to the SP_{aa}, see Fig. 6 and following Fig. 7.

Starting at VRI_{ca}, as well as at a number of other initial nodes, we calculated some SD curves. They are symbolized in Fig. 6 (and in the following Figures) by lines without nodes. The SD coming from a large region around VRI_{ca} goes to the disrotatory minimum M_a (dM_a). The global valley after SP_{ca} leads to the minimum coordinates of dih2 and dih4, thus the rotation of the methylene 1 is turned back and then fixed. The ridge to $(SP_{aa})_{3,5}$ then concerns the coordinates dih3 and dih5. They move "freely" downhill the crest of the ridge, but later turn also to the direction of the disrotatory minimum. Thus, in the classification of refs. [15,56], the VRI region around VRI_{ca} is very lop-sided. It is a skew VRI point, far away from symmetry. It concerns, as well, the lower VRI_{ac}, see below. The SD from there also goes skewly to the disrotatory minimum as it can clearly be seen in the right panel of Fig. 6. The SP_{aa} of Fig. 6 is that one with turned methylene 2. It is named $(SP_{aa})_{3,5}$. The SD for coordinates dih3 and dih5 goes a long part along the ridge, especially for coordinate dih5. Only slightly

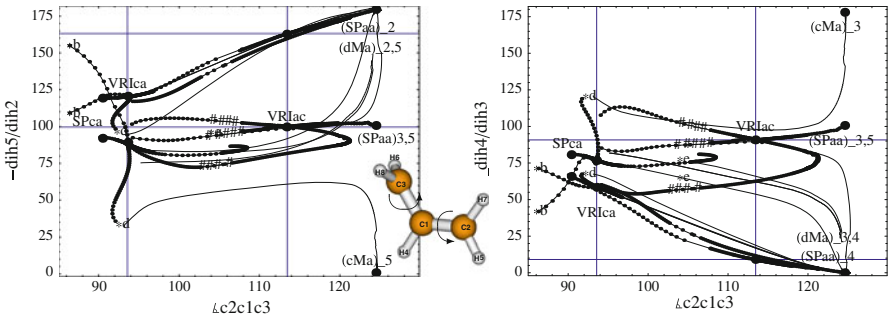

Fig. 6 Ridge from VRI point, VRI_{ca} to SP_{aa}, represented by NTs, see text. *Curves with nodes* are the NTs. *Thin curves without nodes* are SD. *Right*: for coordinates dih3 and −dih4. *Left*: for coordinates dih2 and −dih5. *Left* in the panels is the singular NT of VRI_{ca}. **b*, **d* and **e* are putative CI points. Symbols # depict nodes where the CAS energy did not converge in 50 iterations. The *inlay* is the structure of the SP_{aa} with turned methylene 2. The *arrows* show the conrotatory motion to cM_a which the SD from **d* finds

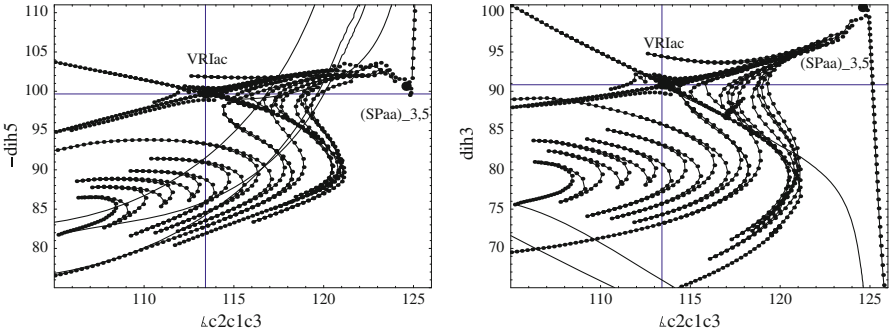

Fig. 7 NTs in an enlarged ridge region around VRI_{ac}. The farthest *left arc* in both panels is the central branch of the singular NT from VRI_{ca}. The wheel of quasi-NTs develops by predictor-only calculations which deviate at strong curved pieces from the true NT. But there is a real TP on every NT. *Right*: for coordinate dih3. *Left*: for coordinate −dih5. The NTs in the *upper part* of the panels are the system of branches through VRI_{ac}. Other *curves without nodes* are SD. *Right* in the panels a regular NT is shown going down to the disrotatory M_a (*outside* the panels) like the SD curves

before the SP_{aa}, the SD turns off and finds its way down to the disrotatory minimum, dM_a. Note that the "ridge" here is a 17-dimensional hyperridge.

Only if we start far away from the VRI_{ca} or the SP_{ca}, for example at the putative CI point, *d, we can get an SD to the conrotatory minimum (cM_a) of the allyl radical. Going to the deflected point *d we overcome the "watershed" of the skew ridge. Thus, it can be guessed that a dynamical trajectory from SP_{ca} should have a certain amount of kinetic energy, to slide over the skew ridge and find the conrotatory minimum [34,35]. But it should be possible. The equipotential hypersurface through VRI_{ca} crosses the SD line from *d before 100° of angle c2c1c3. Note, we found an NT from SP_{ca} in the direction of a pure ring opening which leads to a putative CI point, *e. The ridge way downhill from VRI_{ca} does not touch it, see Fig. 6, if one concerns all dihedrals.

The central branch of the singular NT leaves the VRI_{ca} region downhill as a ridge, and it can be followed by predictor steps, along an Euler-Branin method following the

direction of the vector field **Ag** with Eq. (1). There seems to be a ridge way from VRI_{ca} to SP_{aa}, see Fig. 6. However, the central branch of the singular NT goes downhill to an angle of C2C1C3 of ≈108° but then it has a turning point (TP). It does not reach the SP_{aa}. In Fig. 7 is shown a "family" of quasi-NTs with TPs. It fills the region to a further VRI point, at 113°, which is named VRI_{ac}, to symbolize the transition from the allyl radical bowl to the ridge leading to the SP_{ca}. It is the counterpart to the upper point VRI_{ca} near the SP_{ca}. It corresponds to the VRI_{rl} of part I, see Fig. 13 and Table A5 there. The character is of the mixed type [15,37,56], or a transcritical bifurcation [57]. The two upper branches of VRI_{ac} are ridges of index one. They touch the two lower ridges of index two at VRI_{ac}. This rpVRI point is the bifurcation of the ridge uphill of index one from SP_{aa} which goes further uphill as a ridge of index one into the region of the seam near the putative CI point *d. The ridges of index two below the VRI point border the "TP region". A line of TPs of the former family of NTs is the border between the region with one negative main curvature, and the region with two negative main curvatures around these branches of VRI_{ac}.

All three branches after the bifurcation at VRI_{ac} suffer anywhere on their pathway uphill from a convergence problem of the CASSCF calculation with MAXIT=50. The corresponding nodes are depicted by the symbol # in Fig. 6. Our NT program there uses the former direction, thus, we could continue the curve. But it may be somehow deviated from the "true" shape. Interestingly, the downhill central branch from VRI_{ca} does not suffer from the problem though it seems to be in between the problematic branches. The SD curves do not suffer from the problem either. Note that all NTs and SD curves are calculated in the full-dimensional coordinate space; intersections in the projected 2-dimensional Figs. 6 and 7 are usually not intersections in the full-dimensional space. Of course, the intersection of the four branches of the singular NT through VRI_{ac} is a true intersection in the full-dimensional space.

A further NT is shown downhill from SP_{aa} to the disrotatory allyl-minimum, dM_a, at the right hand side of both panels of Fig. 7. It is the pathway which the SD curves take as well.

The "wavy behavior" of the NTs with TPs only concerns the methylene 2 with the dihedrals 3 and 5 of the hydrogens 6 and 8, correspondingly. It is the methylene which here forms the turned structure of the $(SP_{aa})_{3,5}$. The other methylene 1 is at the minimum value of M_a. The high-dimensional ridge of the PES is very flat, so the corrector of our NT-method does not work there. Larger changes in the coordinates dih3 or dih5 can lead to an equal energy, and an equal NT.

The two systems of branches of the two singular NTs through the VRI points, VRI_{ca} and VRI_{ac}, do not truly fit together, like in part I in the UHF case [37]. (Though the lower dih3-branch of VRI_{ac} touches a version of VRI_{ca}, that is not the right one (it is dih4). If, then it had to go to the upper version in the right panel in Fig. 6, thus also to dih3.) This behavior is also of theoretical importance: obviously there is not exactly one singular NT which connects the two adjacent SPs, SP_{ca} and SP_{aa}. However, there are two singular NTs, and their branches gear into each other. The corresponding branches of one singular NT end at the side walls of the other VRI point as an usual "regular" NT with a TP, and vice versa. The situation is strange, however, it does not violate the index theorem for NTs [58,59] that a regular NT (without a VRI point) cannot connect two stationary points of the same index. Here, we do not have an

NT which fully connects the SP_{ca} with the SP_{aa}. Note: all NTs are "quasi"-NTs. Of course, we lose information if we cannot take advantage of the corrector, especially at curvilinear pieces of the NTs. The calculated curve is built by nodes which are from a family of neighboring NTs. Of course, the global exploration of this ridge region between the SP_{ca} and SP_{aa} is correct. Especially the two VRI points are safe, because usually the central branch of a singular NT is straight, and the calculation of $|\mathbf{Ag}| \approx 0$ does not depend on the corrector. Also the incidentally found CI points on any seam are not depend on a corrector step.

6 Exploration of pathways from SP_{ca} to a conrotatory ring opening

6.1 Direct NTs to $(SP_{aa})_{2,4}$

A pathway should exist from SP_{ca} to the alternate $(SP_{aa})_{2,4}$ where the methylene 1 is still turned, but the methylene 2 is in the plane of the C-atoms, compare the inlay in Fig. 8. The direction is a different degree of freedom of the coordinates space than the direction to $(SP_{aa})_{3,5}$ treated in Figs. 6 and 7. If the connection is throughout a ridge then we do not need the existence of a VRI point in between. However, corresponding to the index theorem for NTs [58,59], we find then an SP of index two on the pathway in between: it is here replaced by a CI point. We found indeed NTs which connect the two SPs without a VRI point. They may be treated as representants of the family of infinitely many of such NTs. However, as anticipated, there is always a crossing of a seam. Such NTs should be a leading line of a conrotatory ring opening. The main valley connected with $(SP_{aa})_{2,4}$ is here the minimum bowl of M_a for coordinates of dih3 and dih5 which are at the allyl radical values, thus the rotation of the methylene 2 is now turned back and fixed: from the values of SP_{ca} to 0° for dih5, and to 180° for dih3. The ridge to $(SP_{aa})_{2,4}$ concerns the coordinates dih2 and dih4. After the CI point they move "freely" downhill the crest of the ridge, but then usually turn to the conrotatory direction. The pathway is a little more energetic than the ridge to

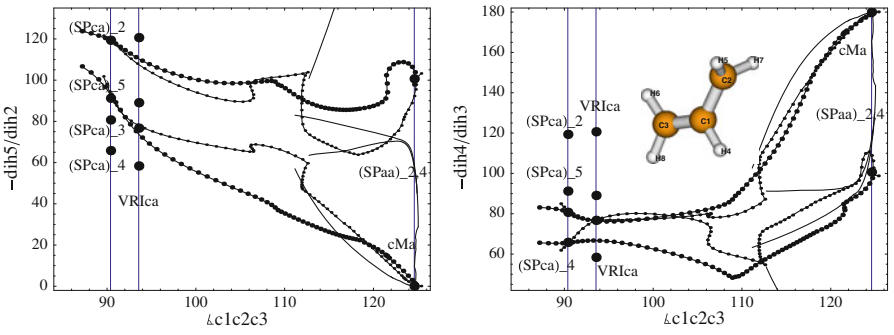

Fig. 8 Two NTs in the ridge region from SP_{ca} to the other $(SP_{aa})_{2,4}$. There is a change in the two methylenes: the result is a more stable conrotatory pathway to the allyl radical minimum. *Right*: for coordinates dih3 and −dih4. *Left*: for coordinates dih2 and −dih5. NTs are *curves with nodes*, other *curves without nodes* are SDs. The *inlay* is the geometry of $(SP_{aa})_{2,4}$

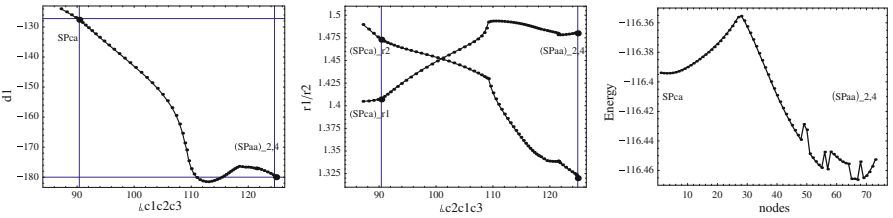

Fig. 9 NT with fat nodes of Fig. 8 in the ridge region from SP_{ca} to the other $(SP_{aa})_{2,4}$. *Left*: for coordinate dih1. *Center*: for coordinates r1 and r2. *Right*: energy profile

$(SP_{aa})_{3,5}$ because the distances r_1 and r_2 have to change their order, see the central panel in Fig. 9. (Figure 9 concerns the one NT of Fig. 8 with the fat nodes.)

The two SPs, SP_{ca} and $(SP_{aa})_{2,4}$, are connected over a ridge of the PES. Because the two versions $(SP_{aa})_{2,4}$ and $(SP_{aa})_{3,5}$ are symmetric, they must have the same energy. However, the SP_{ca} is unsymmetric, and so the two connections are different, also in energy. Figure 8 shows the dihedrals of the methylene groups, and Fig. 9 shows further coordinates. The NTs only need little more energy than for overmounting the SP_{ca} at all. The energy profile of the NT with the fat nodes of Fig. 8 is given in Fig. 9 in the right panel. (Compare the amount of ≈ 0.03 au over the SP_{ca}-energy with results of the next Sect. 7.) In the left panel of Fig. 9 we additionally represent the dihedral dih1 of the methine group. The SP_{aa} needs a value of $-180°$ which is indeed realized. The NTs have a kink: this one with fat nodes at $\approx 109°$, the other one at 112°. There they probably cross a seam of an electronic intersection. Because we only use "quasi-NTs", meaning NTs calculated by only predictor steps, the crossing of a seam happens without problems. The next predictor step after the seam uses the new $\mathbf{A}\,\mathbf{g}$ direction with Eq. (1). If we find a kink in such a quasi-NT, we can guess that a seam is crossed.

Starting the SD at two different initial nodes on the ridge to $(SP_{aa})_{2,4}$ gives the cM_a bowl (the usual case), or the dM_a bowl (the seldom case), correspondingly, quite in the alternate situation to the region of the $(SP_{aa})_{3,5}$. Again, a skew watershed character of the ridge to $(SP_{aa})_{2,4}$ emerges.

The unsteady energy profile near SP_{aa} in the right panel of Fig. 9 is caused by jumps of the CASSCF(3,3) method between different electronic surfaces. However, the question of a con- or disrotatory behavior is not directly concerned with that problem. So we do not discuss it further here.

6.2 Singular NT through $(VRI_{ac})_{2,4}$

In this subsection we explore a direction of the configuration space which was not taken into account in paper I [37]. It concerns pathways from the central SP_{ca} of the ring opening to another symmetry form of the SP_{aa}, the $(SP_{aa})_{2,4}$ where methylene 1 is turned, but not methylene 2. Such pathways skew downhill over a skew ridge. They are very skew to the level hypersurfaces of the PES, and thus they are so-called non-IRC-curves. That is the reason that they cannot well explored by stepest descent methods only. However, NTs are a good tool to explore such pathways. Interestingly,

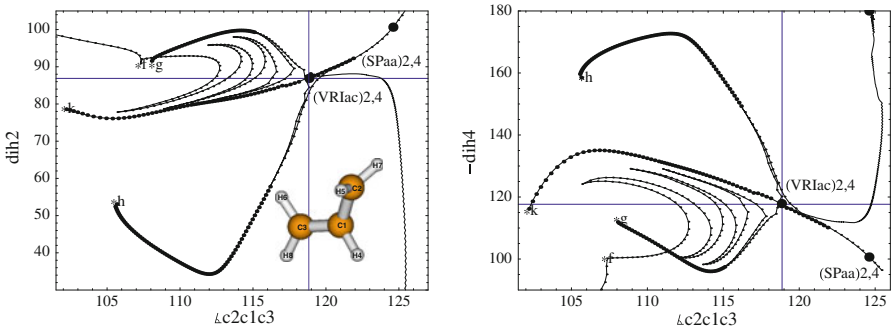

Fig. 10 Singular NT (*fat nodes*) from SP_{aa} through the $(VRI_{ac})_{2,4}$. An exploring quasi-NT is shown by *thin nodes*. The *curve without nodes* is the SD from the VRI point. All branches after the VRI point lead to putative CI points, *g, *h and *k. *Right*: for coordinate −dih4. *Left*: for coordinate dih2. The *inlay* is the geometry of $(VRI_{ac})_{2,4}$

this kind of reaction paths leads mainly to the other bowl of the allyl radical minimum, the conrotatory one.

Looking on the VRI point, $(VRI_{ac})_{3,5}$, near the $(SP_{aa})_{3,5}$ one should expect by symmetry reasons that there is also a similar VRI point near $(SP_{aa})_{2,4}$. We could find one, see Fig. 10 and Table 4. It is named $(VRI_{ac})_{2,4}$. It is remarkable that it is moved somehow from its former place concerning the angle of the ring opening. Its central branch leads uphill from $(SP_{aa})_{2,4}$. It is a ridge. The character of the bifurcation is an rpVRI: the ridge of index one from SP bifurcates into two outer ridge forks of index one, and the central fork is a valley in between going also uphill. All three branches lead after the bifurcation to putative CI seam points, depicted in Fig. 10 by *g to *k. The CI point *h is very "strong". Its value $|\mathbf{Ag}|$ is 3,925,000, and the first eigenvalue of the Hessian is −24.486 (the transversal curvature of the seam), its second eigenvalue is −0.24, (the longitudinal curvature). The point *g has $|\mathbf{Ag}| = 12658$, and the point *k is "mild" with $|\mathbf{Ag}| = 350$. Its transversal curvature is −0.317, its longitudinal curvature is −0.0026, thus it is quite flat. We found the VRI point by an "exploring" quasi-NT with thin nodes, coming from the left region of SP_{ca} (it is not shown in the panels). After the putative CI point *f, the curve goes into a wheel of quasi-NTs, as well as the exploring quasi-NT in Fig. 6. The fan is a hint to a curve of TPs, a border of valley- and ridge regions of the PES. And indeed, the branch to point *k is a valley line, where the branch to point *g is a ridge line.

The existence of the $(VRI_{ac})_{2,4}$, as well as of the $(VRI_{ac})_{3,5}$, demonstrates that the ridge over SP_{aa} is not a surface with a single, global curvature. However, the ridge will be divided by ribs and rills, like the sandheap in Fig. 1.

7 Exploration of pathways from SP_{ca} back to SP_{ca} in an alternate symmetry

The Czech mountains "High Tatra" are surrounded by a flank way which holds quasi always the same level: the "tourist magistrala". It is an easy-going pathway. On the way one could find the initial point to the climbing path uphill to any summit, as well as

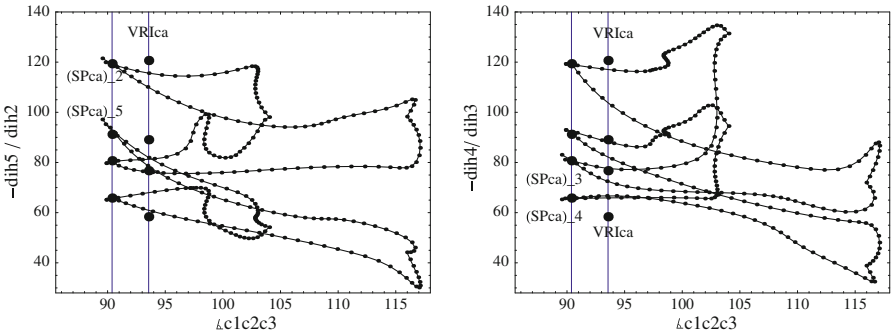

Fig. 11 Two quasi- NTs in the ridge region after SP_{ca}. There is a change in the two methylenes. *Right*: starting with coordinates dih3 and −dih4, but ending with the other two. *Left*: starting with coordinates dih2 and −dih5, but ending with the other two

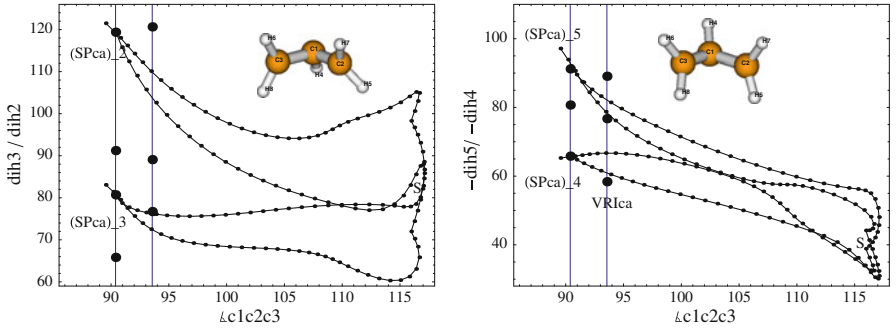

Fig. 12 The more extended quasi-NT of Fig. 11 in the ridge region after SP_{ca} representing a symmetry change of the SP_{ca}. *Right*: coordinates −dih4 and −dih5. *Left*: coordinates dih2 and dih3. Symbol *S* is the crossing point of the coordinates. The *inlay* in the *left panel* is the SP_{ca} in the representation here used with $r_1 < r_2$ and the dihs 2 and 5 are larger than dihs 3 and 4, see Table 1. The *inlay* in the *right panel* is the other symmetric form, see text

an initial point to go down to any valley. Such a roundabout pathway we could identify also on the PES behind the SP_{ca}. It connects one form of the SP_{ca} with another form where the asymmetry of the dihedrals is exchanged. On the long way through the PES mountains it holds a quasi equal level. But like from the "tourist magistrala", one can go downhill from different points of the way to different valley versions of the allyl radical minimum.

We found quasi-NTs which start at SP_{ca} and go across the ridge in the direction to $(SP_{aa})_{2,4}$ but at ≈104°, or at ≈117° of the reaction coordinate, they return to another SP_{ca} symmetry. For example the coordinates of the NT starting at SP_{ca}, dih2 and dih5, return to coordinates dih3 and dih4 of the SP_{ca}, and vice versa. That realizes a symmetry exchange in relation to dih1 and the CCC-plane, see Figs. 11 and 12. The energy amount is nearly the same like to find the way to SP_{aa} in Sect. 6.

The more extended NT is shown again in Fig. 12 in a representation where the dihedrals are sorted in a different kind. There one can detect the crossing point of the mutual symmetric coordinates, by the symbol 'S' like symmetry. The distances r1 and r2 also

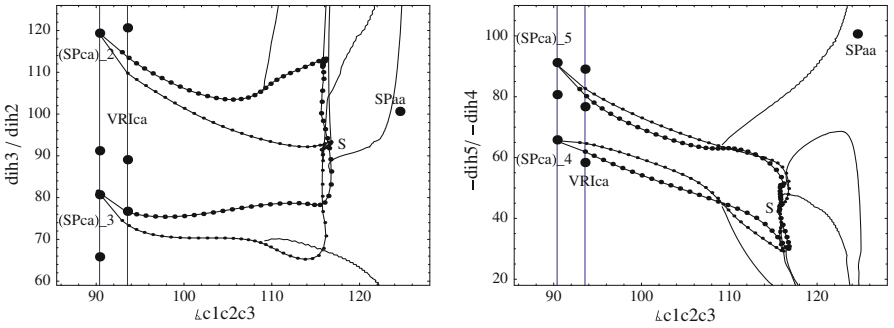

Fig. 13 Result of a "nudged band" calculation: a chain of nodes in the ridge region after SP_{ca} with a symmetry change of the SP_{ca}. Symbol *S* (like symmetry) is the crossing point of the coordinates. *Curves without nodes* are SD, see text. *Right*: coordinates −dih5 and −dih4. The chain with *fat nodes* starts at $(SP_{ca})_5$ and ends at $(SP_{ca})_4$; *thin nodes* are the complement. *Left*: coordinates dih2 and dih3. *Fat nodes* start at $(SP_{ca})_2$ and end at $(SP_{ca})_3$; *thin nodes* are the complement

cross along the pathway of the NT, and the dihedral dih1 of the methine group goes through the CCC-plane with −180°. However, the four symmetry events happen at different nodes along the reaction coordinate. dih1 crosses −180° at C2C1C3 angle of ≈109.5°, r1 and r2 interchange at ≈116.1°, dih4 and dih5 interchange at ≈116.3°, and dih2 and dih3 interchange at ≈117.1°. The NT avoids the fully symmetric subspace; the interchangings always happen in 2-dimensional subspaces only.

The NT represents a change in the symmetry of the SP_{ca}. Going from the initial to the final node, it is a rotation, C_2, around an axis through C1 atom lying in the CCC-plane. The rotational axis is the bisecting line of the angle between the C-atoms. After the rotation, the methylenes are renumbered: C2 and C3 are to be renumbered, and the H-atoms of the methylenes are renumbered also: H5 and H6 interchange, and H7 and H8 interchange, as well. The two different numbered forms represent one and the same structure. They should not influence the question of the con- or disrotatory ring opening. In contrast, we find that an SD line touches different versions of the SP_{aa} depending on the initial node. One version of the SD goes to the $(SP_{aa})_{3,5}$, the other to $(SP_{aa})_{2,4}$. However, the NTs of Fig. 11 represent continuous changes of the molecule, mainly of the coordinates r1 and r2, and the dihedrals 2–5. The orbitals of the electrons can not follow that pathway in a continuous kind, compare Fig. 4. Thus, an intersection has to take place on the way, and we found it on every NT of this kind.

One could ask for the energy amount to reach the SP_{aa} region by such a roundabout chain. Maybe there is a chain which has not to overcome an additional energy after SP_{ca}? To prove that we make a kind of a "nudged band" calculation. We drop the energy of every node of the NT. We use the gradient direction at the current node, and additionally weight a step length factor by the difference of the current energy with the energy of the SP_{ca}. The result (after 24 iteration loops) is represented in Figs. 13 and 14. Because one has to cross a seam, the new chain of such nodes is hanging at the seam, as well, like the NT of Figs. 11 and 12. The result now is a fixed, and quasi symmetric chain in the coordinate pairs r1, r2, and dih2, dih3, and dih4, dih5,

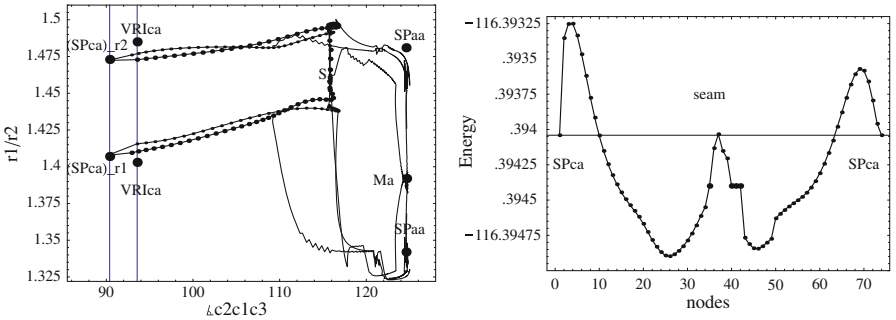

Fig. 14 The chain of Fig. 13 for *Left*: coordinates r1 and r2. *Fat nodes* start at SP_{ca} as r1 and end back as r2; *thin nodes* are the complement. *Curves without nodes* are SD. They touch any version of the SP_{aa}, see text. *Right*: energy profile along the chain; it is quite flat

correspondingly. The two coordinates r1, r2 interchange at the seam, but the other coordinates interchange at different nodes, as before on the NT. The pathway does not change in further iterations. It is clearly divided in three parts: one region where r1 > r2, the other where r1 < r2, and the r_i stay nearly constant along the ring opening, they only a little increase there, and a third part where the ring angle is constant, but the r_i changes the value. (The dihedrals dih_i, $i = 2, \ldots, 5$ behave analogously.)

In Figs. 13 and 14, additional curves without nodes are three SD calculations. One starts before the equality, one at the r1 = r2 node, and the last after the equality.

The SD calculations are clearly different:

– two touch the $(SP_{aa})_{2,4}$, for start at ≈117° angle, and r1 > r2 , or r1 = r2, there dih3 rises up to 180°, dih5 falls down to 0°, but dih2/dih4 touch the SP_{aa}.
– one touches the $(SP_{aa})_{3,5}$, for start at ≈109° angle, r1 < r2, and there dih2 rises up to 180°, dih4 falls down to 0°, but dih3/dih5 touch the SP_{aa}.

The energy profile of the chain is quasi "flat" at the SP_{ca} level, see Fig. 14, right panel. There are four nodes (nodes 35, and 40 to 43, fat bullets in figure) which are on the r_i exchange part, where the CASSCF(3,3) algorithm does not converge in 50 iterations, thus the energy is missing there. We use an average value. The central 'peak' (node 37 of the chain) is clearly near to a seam point, there the |**Ag**|-value goes: …, up, …, 731, 1127, 752, …, down, …

8 An additional exploration of the former SP_{d1} on the UHF surface

In this section we represent a VRI point in the region of the very interesting SP_{d1} on the former UHF surface of the allyl radical, see paper I [37]. Here, the transition to the CASSCF(3,3) method changes qualitatively the character of the PES. The SP of index one disappears, but a usual VRI point emerges. The pathways of Sects. 5 and 6 show a drift apart from the dihedrals 2 and 5, as well as the dihedrals 3 and 4: one sort stays at the value of the SP_{ca} to fit the values of one turned methylene at $(SP_{aa})_{3,5}$, or at $(SP_{aa})_{2,4}$ correspondingly. The other sort tends to the minimum value of the allyl radical, being the flat structure of the other methylene of the SP_{aa}.

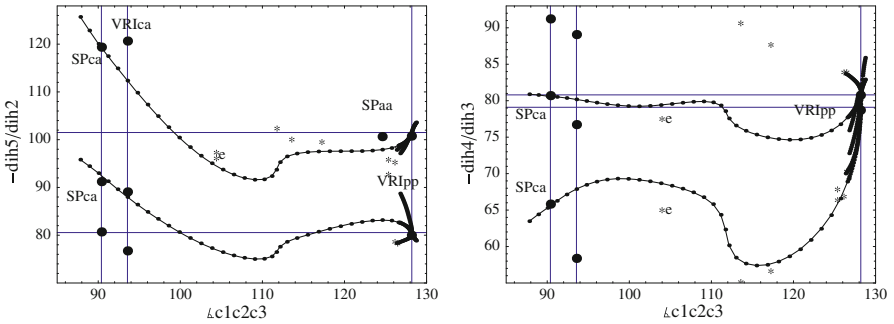

Fig. 15 Singular NT from SP_{ca} to VRI_{pp}. *Right*: for coordinates dih3 and −dih4. *Left*: for coordinates dih2 and −dih5. The location of the SP_{aa} is only in the used projection nearby for coordinate dih2. The putative CI point $_*$e is the same like in Figs. 4 and 5. Symbols $_*$ *without a letter* are further seam points

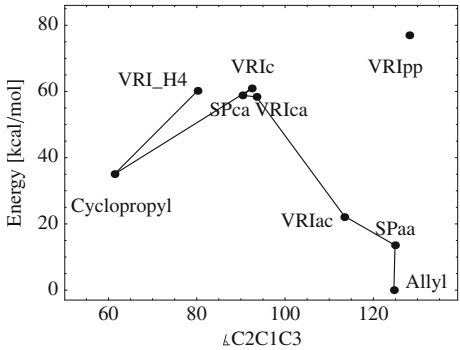

Fig. 16 Energies of diverse points for the cyclopropyl radical ring opening

Here, we report another pathway starting at SP_{ca} as well, but showing a quasi parallel behavior of the dihedrals 2–5 along a long way of a quasi pure ring opening, to a further, new VRI point. It is named VRI_{pp}, see Fig. 15. Here, symbol 'pp' is used for parallel pathway.

This VRI point replaces the role of the SP_{d1} of the UHF surface, see part I. The former VRI_r here seems not to exist. The pathway from SP_{ca} to VRI_{ca}, Figs. 6 and 7, is the groundway of a valley. The new NT from SP_{ca} to VRI_{pp} starts along the slope of the SP_{ca} as a ridge way slowly uphill. The energy profile goes somehow over the level of the SP_{ca}, see Fig. 16. The amount of energy here is again used to interchange both distances, r1 and r2, at ≈103° of the ring angle. A dynamical trajectory may go through the region, to coarsely follow the NT to VRI_{pp}. Of course, a "relaxation" from the region of VRI_{pp} to SP_{aa} is possible; we obtained corresponding NTs. But the VRI point is possibly too high in energy to be of interest for the con- or disrotational question. The Sects. 6 and 7 have opened deeper pathways to the allyl minimum in both rotational directions. Due to this fact we stop the discussion at this point.

At the end, we represent the energies of the different points discussed in the paper in Fig. 16. Most of the NTs of the Sects. 6, 7, and 8 move in the energy region lower than the energy of VRI_{pp}.

9 Conclusion

NTs open a cornucopia of insights into the structure of the PES. Of course, to get the NTs reported here, we had to test a somehow greater number of them. Concerning the search direction, the parameter which determines every NT [8,9], there applies a sentence of Leonhard Euler: "Science is what you do after you guess well." Then NTs solve the question concerning the cyclopropyl PES formulated in ref.[34,35]. There classical dynamics is done with 100 trajectories, but the con- or disrotatory question could not be solved. The authors could only ascertain that the conrotatory minimum is also often reached. Now the Newton trajectory method gives an explanation: There are static NTs which connect the global SP of the ring opening with the disrotatory minimum, as well as also with the conrotatory one. In this way this work gives an example for the utility of the Newton trajectory method in a real chemical problem. Because, if there are static pathways of low energy between the corresponding bowls, one can assume that also dynamical trajectories can find their way there.

The lowest electronic CASSCF-PES for the ring opening of the cyclopropyl radical is notoriously curvilinear. To see anything at all, we concentrate our imagination to projections to the 5 dihedrals, and the two distances of the C-atoms of the 8-atomic molecule. So we move in our imagination in an 8-dimensional space, with the 3-dimensional 'dividing' subspace of full symmetry, though we calculate the one-dimensional NTs in the full 18-dimensional configuration space. But 8 degrees of freedom are by far enough to hide important aspects of the PES, possibly. With this work, we continue the possibility to channelize the ring opening of the cyclopropyl radical on the PES between some singular NTs. The known SP of the ring opening, SP_{ca} [32], is connected to a row of VRI points. The tool to find these special points is a good guess, and then a variational application of Newton trajectories proposed in ref. [24]. For the guess of diverse VRI points on the CAS surface it was very helpful to employ the results of the UHF surface [37].

After the SP_{ca} of the ring opening, and before the adjacent $(SP_{aa})_{3,5}$ in the allyl bowl, has to be at least one further VRI point. We propose to assume the VRI_{ca} for that event. However, its central branch does not lead downhill directly to the SP_{aa}. Rising from SP_{aa}, on the other hand, we found a further VRI point of the mixed rpVRI character of higher index. But also its singular NT does not directly lead to SP_{ca}. But the systems of the singular NTs of that VRI points describe the ridge region where one can guess the pathway of the ring opening. The singular NTs through the VRI points mark a border for such RP models marking a so-called reaction channel [17,59,60] of NTs. It is further demonstrated by different SD calculations, at least, which find their way through the different singular NTs. These set the limits for the SD form SP_{ca} to dM_a, the disrotatory allyl radical minimum. A local variation of the initial point of an SD does not change the result. There is not known any IRC calculation which could explain that the conrotatory minimum can emerge. But the downhill SD on a ridge is usually 'instable'. A larger 'shift' of the pathway along an equipotential hypersurface could lead to the other minimum, cf. Fig. 5 of ref. [4].

A second possibility, still not detected in part I, is a pathway from SP_{ca} along the other ridge to $(SP_{aa})_{2,4}$. That ridge ends at an equal energy height like $(SP_{aa})_{3,5}$, because both are symmetric. But the direction in the configuration space is another

one. And because the distances r_1 and r_2 have to cross along that ridge, its connection is different from the $(SP_{aa})_{3,5}$ case. The connecting NTs cross a seam. After that, the ridge pathways downhill to $(SP_{aa})_{2,4}$ mainly lead to the conrotatory M_a minimum bowl.

We can report a third kind of chains, roundabout pathways from SP_{ca} and back in another symmetric configuration. The chains hold an equal level of energy. To go down to the con- or disrotational bowl of the allyl radical is again possible starting on such ways.

On the PES we found a world of CI seam points going criss cross over wide regions. Some doorways through such seams are reported. A more extended representation of seams is not given here. It is moved in another paper [54]. We think that the combination of singular NTs and of the diverse seams will be a representative picture of the interesting regions of the PES.

The use of SD separates the different interesting points of the PES (SPs, VRI points) into different catchment regions of the dis- or conrotatory minimums, see [1,61]. Globally, there are the two main channels. But the ring opening shows a possibility of the mixed character of con- and disrotatory motion of the methylenes if one traces the different singular NTs, as well as the SD for accessible regions after the SP_{ca}. The summary result of NTs or SD from SP_{ca} down the SP col is the disrotatory minimum. However, the singular NT along a ridge region from SP_{ca} to $(SP_{aa})_{2,4}$ could explain a channel for a mainly conrotatory ring opening. Of course, IRC and NTs are static pathways. They are not dynamical trajectories. Thus, the static pathways given in this work are not comparable directly with the constant energy dynamics [34,35]. However, we assume that doorways through the energy mountains found by NTs could also be used by the dynamical trajectories with the corresponding energy. The diverse singular NTs set the limits for usual static reaction pathways on the PES. But they may open the insight for results of dynamical trajectories [34,35], where the relation of trajectories to a conrotatory against a disrotatory ring opening is halves. With the reaction of the cyclopropyl radical ring opening to the allyl radical we have shown that the NT methodology provides a tool to explore the topology of the potential energy surface [9]. The so-called singular Newton trajectories acquire special importance. These curves pass through the VRI points and the corresponding analysis of each branch that crosses the VRI provides information on the structure and form of the surface around this point. They are related to the bifurcation of valleys.

Acknowledgments Financial support from the Spanish Ministerio de Ciencia y Tecnologia, DGI project CTQ2011-22505 and, in part from the Generalitat de Catalunya projects 2009SGR-1472 is fully acknowledged. We thank the referees for suggestions and helpful comments.

References

1. P.G. Mezey, *Potential Energy Hypersurfaces* (Elsevier, Amsterdam, 1987)
2. D. Heidrich (ed.), *The Reaction Path in Chemistry: Current Approaches and Perspectives* (Kluwer, Dordrecht, 1995)
3. K. Fukui, J. Phys. Chem. **74**, 4161 (1970)
4. P.G. Mezey, Theor. Chim. Acta **54**, 95 (1980)
5. W. Quapp, D. Heidrich, Theor. Chim. Acta **66**, 245 (1984)

6. M. Hirsch, W. Quapp, Chem. Phys. Lett. **395**, 150 (2004)
7. I.H. Williams, G.M. Maggiora, J. Mol. Struct. (THEOCHEM) **89**, 365 (1982)
8. W. Quapp, M. Hirsch, D. Heidrich, Theor. Chem. Acc. **100**, 285 (1998)
9. W. Quapp, M. Hirsch, O. Imig, D. Heidrich, J. Comput. Chem. **19**, 1087 (1998)
10. W. Quapp, J. Comput. Chem. **22**, 537 (2001)
11. M. Hirsch, W. Quapp, J. Comput. Chem. **23**, 887 (2002)
12. J.M. Anglada, E. Besalu, J.M. Bofill, R. Crehuet, J. Comput. Chem. **22**, 387 (2001)
13. J.M. Bofill, J.M. Anglada, Theor. Chem. Acc. **105**, 463 (2001)
14. R. Crehuet, J.M. Bofill, J.M. Anglada, Theor. Chem. Acc. **107**, 130 (2002)
15. W. Quapp, J. Mol. Struct. **695–696**, 95 (2004)
16. Y. Liu, S.K. Burger, P.W. Ayers, J. Math. Chem. **49**, 1915 (2011)
17. M. Hirsch, W. Quapp, J. Math. Chem. **36**, 307 (2004)
18. J.M. Bofill, W. Quapp, J. Chem. Phys. **134**, 074101 (2011)
19. H. Hirsch, W. Quapp, D. Heidrich, Phys. Chem. Chem. Phys. **1**, 5291 (1999)
20. W. Quapp, V. Melnikov, Phys. Chem. Chem. Phys. **3**, 2735 (2001)
21. W. Quapp, D. Heidrich, J. Mol. Struct. (THEOCHEM) **585**, 105 (2002)
22. K. Müller, L. Brown, Theor. Chim. Acta **53**, 75 (1979)
23. F.H. Branin, IBM J. Res. Dev. **16**, 504 (1972)
24. W. Quapp, B. Schmidt, Theor. Chem. Acc. **128**, 47 (2011)
25. GAMESS-US program: M.V. Schmidt, K.K. Baldridge, J.A. Boatz, S.T. Elbert, M.S. Gordon, J.H. Jensen, S. Koseki, N. Matsunaga, K.A. Nguyen, S. Su, T.L. Windus, M. Dupuis, J.A. Montgomery Jr., J. Comput. Chem. **14**, 1347 (1993)
26. GAMESS-US program: M.S. Gordon, M.W. Schmidt, in Theory and Applications of Computational Chemistry, the First Forty Years, ed. by C.E. Dykstra, G. Frenking, K.S. Kim, G.E. Scuseria (Elsevier, Amsterdam, 2005), Chap. 41, p. 1167. GAMESS V 2007
27. GAMESS-US program: A.A. Granovsky, Firefly Project: http://classic.chem.msu.su/gran/firefly (2009)
28. W. Quapp (2010) web-page: www.math.uni-leipzig.de/~quapp/SkewVRIs.html
29. R.B. Woodward, R. Hoffmann, J. Am. Chem. Soc. **87**, 395 (1965)
30. R.B. Woodward, R. Hoffmann, Angew. Chem. Int. Ed. Engl. **8**, 781 (1969)
31. D.T. Clark, D.B. Adams, Nat. Phys. Sci. **233**, 121 (1971)
32. S. Olivella, A. Solé, JM Bofill, J. Am. Chem. Soc. **112**, 2160 (1990)
33. P.A. Arnold, B.K. Carpender, Chem. Phys. Lett. **328**, 90 (2000)
34. D.J. Mann, W.L. Hase, J. Am. Chem. Soc. **124**, 3208 (2002)
35. D.J. Mann, M.D. Halls, Phys. Chem. Chem. Phys. **4**, 5066 (2002)
36. A. Aguilar-Mogas, X. Giménez, J.M. Bofill, J. Comput. Chem. **31**, 2510 (2010)
37. W. Quapp, J.M. Bofill, A. Aguilar-Mogas, Theor. Chem. Acc. **129**, 803 (2011)
38. K. Ruedenberg, W. Schmidt, M.M. Gilbert, S.T. Elbert, Chem. Phys. **71**, 41 (1982)
39. B.O. Roos, P.R. Taylor, P.E.M. Siegbahn, Chem. Phys. **48**, 157 (1980)
40. H.-J. Werner, Adv. Chem. Phys. **69**, 1 (1987)
41. R. Shepard, Adv. Chem. Phys. **69**, 63 (1987)
42. B.O. Roos, Adv. Chem. Phys. **69**, 399 (1987)
43. P. Pulay, T.P. Hamilton, J. Chem. Phys. **88**, 4926 (1988)
44. J.M. Bofill, P. Pulay, J. Chem. Phys. **90**, 3637 (1989)
45. S. Wilsey, J. Org. Chem. **65**, 7878 (2000)
46. C. Cramer, *Essentials of Computational Chemistry* (Wiley, Chichester, 2004)
47. D.R. Yarkony, Rev. Mod. Phys. **68**, 985 (1996)
48. T.J. Martinez, Nature **467**, 412 (2010)
49. G.J. Atchity, S.S. Xantheas, K. Ruedenberg, J. Chem. Phys. **95**, 1862 (1991)
50. G.J. Atchity, K. Ruedenberg, J. Chem. Phys. **110**, 4208 (1999)
51. K. Holtzhauer, C. Cometta-Morini, J.F.M. Oth, J. Phys. Org. Chem. **3**, 219 (1990)
52. F. Dong, S. Davis, D.J. Nesbitt, J. Phys. Chem. **110**, 3059 (2006)
53. W. Quapp, J. Theor. Comput. Chem. **2**, 385 (2003)
54. W. Quapp, J.M. Bofill (2012) Chem. Phys. Lett. (submitted)
55. J.M.T. Thompson, H.B. Stewart, Y. Ueda, Phys. Rev. E **49**, 1019 (1994)
56. W. Quapp, M. Hirsch, D. Heidrich, Theor. Chem. Acc. **112**, 40 (2004)
57. C. Kuehn, Physica D **240**, 1020 (2011)

58. I. Diener, *Globale Aspekte des kontinuierlichen Newtonverfahrens*. Habilitation, Universität Göttingen (1991)
59. M. Hirsch, W. Quapp, J. Mol. Struct. (THEOCHEM) **683**, 1 (2004)
60. W. Quapp, J. Theor. Comput. Chem. **8**, 101 (2009)
61. P.G. Mezey, Int. J. Quant. Chem. **29**, 333 (1986)